Assessment of Axial Cracking of a Steam Generator Tube

G. Sanyal[1], M. K. Samal[2]

[1]Mechanical Metallurgy Division, [2]Reactor Safety Division, Bhabha Atomic Research Centre
Trombay, Mumbai-400085, India

[1]gsanyal@barc.gov.in; [2]mksamal@yahoo.com

Abstract- **Steam generator (SG) tubes are extensively used in the form of thin-walled tubular structural members as heat exchangers for generation of steam in order to convert thermal energy to electricity in nuclear power plants. These tubes are exposed to aggressive environments such as high temperature, internal pressure and flow-induced vibration etc. Since at present no standard test procedure can guarantee accurate quantification of axial crack resistance of such tubes because of their unusual geometry, the present work attempts structural integrity assessment of an SG tube using a new method called pin loading tension test (PLT) as has been done by the authors for fuel cladding tubes fabricated with zirconium alloys in recent past. The current work involves experimental and analytical derivation of various geometric functions required for calculation of stress intensity factor (SIF) and J integral. Using the derived functions, J-R curve for an axially cracked SG tube made of Ni-Cr-Fe based alloy used in power plants of Indian pressurized Heavy Water Reactors (PHWR) is calculated. Also, the characterization of fracture surface by SEM fractography is done to predict suitable cracking mechanism.**

Keywords- SG Tube; Incoloy-800; J-R Curve; Load Normalization Technique; Fractograph

I. INTRODUCTION

A steam generator is a device that uses a heat source to boil liquid water and convert it into its vapour phase, i.e. steam. The heat may be derived from the combustion of a fuel such as coal, petroleum fuel oil, natural gas, municipal waste or biomass, a nuclear fission reactor or other sources. There are many different types of steam generators ranging from small medical and domestic humidifiers to large steam generators used in conventional coal-fired power plants that generate about 3,500 kilograms of steam per megawatt-hour of energy production. Pressurized water reactors (PWRs) use steam generators [1], which convert water into steam using heat produced in the nuclear reactor core. These devices can measure up to 70 feet in height and weigh as much as 800 tons. Inside the steam generators, hot radioactive water is pumped through thousands of feet of tubing–each steam generator can contain anywhere from 3,000 to 16,000 tubes, each about three-quarters of an inch in diameter–under high pressure to prevent it from boiling. That water flowing through the inside of the tubes then heats non-radioactive water on the outside of the tubes. This produces steam that turns the blades of turbines to make electricity. The steam is subsequently condensed into water and returned to the steam generator to be heated once again. These tubes have an important safety role because they constitute one of the primary barriers between the radioactive and non-radioactive sides of the plant. Hence, the integrity of the tubing is essential in minimizing the leakage of water between the two "sides" of the plant. There is the potential that if a tube bursts while a plant is operating, radioactivity from the primary coolant system–the system that pumps water through the reactor core–could escape directly to the atmosphere in the form of steam. Thus, for ensuring longer uninterrupted hassle-free plant operation, it is required to carry out inspection, repairing of the tubes and monitoring of water chemistry to detect radiation leaking from the primary to the secondary side of the plant. Additionally, fabrication route of the tubes has to be such that the tubes must have an extremely low probability of abnormal leakage.

Earlier generation nuclear power plants employed steam generators having Monel-400 as the tube material. This alloy was noticed prone to stress corrosion cracking under high dissolved oxygen concentration of the coolant and also showed higher rate of general corrosion resulting in release of cobalt-59 (present as an impurity with nickel in the alloy) which generated a highly radioactive species, cobalt-60, on irradiation with the thermal neutrons. It resulted in a higher radiation dose to operation & maintenance personnel working in these PHWRs. Therefore, Monel-400 was replaced with alloy-600 (Inconel-600) in some reactors across the world. As this alloy was also found to be failing through inter-granular stress corrosion cracking (IGSCC), India chose to employ a better alloy [2], i.e. Incoloy-800. This material has demonstrated a high resistance to general corrosion, especially under high dissolved oxygen concentration of the coolant (>100ppb), and IGSCC. Nickel content in this alloy is low, therefore cobalt-59 associated with this material is nearly absent (30 wt% in Incalloy-800 vis-à-vis 70 wt% in Monel-400). The low corrosion rate of Incoloy-800 and absence of cobalt-59 has eliminated the problem of cobalt-60 generation in PHWRs. This has lead to reduction in radiation field on the out of core equipment surfaces where maintenance activities are undertaken.

During service time, various corrosion assisted degradation mechanisms are found to cause different types of failure of SG tubes across the world. A few major phenomena are briefly discussed below for considering the importance of structural integrity of SG tube. Primary Water Stress Corrosion Cracking (PWSCC) [3-6] occurs most commonly in the tube expansion transition region, or roll transition zone (RTZ), where the tube is expanded into the tube sheet. The cracks are usually axial, but circumferential cracking has also been observed and can occur near the end of the expanded region above the tube sheet or farther down in the expanded portion of the tube. The forming processes used to produce U-bends [7, 8] in steam generator tubes can create residual stresses in the bends, with the greatest stress levels occurring in the inner row tubes with the smallest radius of curvature. These stresses, in combination with a susceptible microstructure, can be sufficient to cause PWSCC problems. PWSCC has also been known to initiate at tube dents resulting from tube support plate (TSP) corrosion [9].

PWSCC can also occur in the plugs used to remove steam generator tubes from service [10-11]. PWSCC of tube regions fitted with repaired sleeves is also reported in the literature [12-13]. Cracking typically occurs not in the sleeve itself, but in the tube material adjacent to one of the sleeve welds. Outer Diameter Stress Corrosion Cracking (ODSCC) is another leading cause of PWR steam generator tube plugging and the tube support plate crevice is the predominant location for this process. Corrosion products, mainly from the tube support plate, and deposited sludge from the secondary water system eventually fill this crevice with porous material, resulting in a region of restricted secondary water flow, intermittent dry-out, and concentration of corrosive species. The pH of the concentrated crevice may be very basic if the bulk water has a high cation/anion ratio or somewhat acidic for a low cation/anion ratio [14]. The OD cracking observed in the tube support plate crevice is generally intergranular in nature and commonly consists of short axial cracks of varying length and depth within the crevice region. Adjacent cracks are often separated by ligaments of sound tubing material, and crack linkage can occur as ligament sections are corroded. ODSCC and intergrannular attack (IGA) also commonly occur in the tube sheet region, either in the built-in crevice between the tube sheet and the tubes that was present in earlier Westinghouse designs [7] or in the sludge pile atop the tube sheet. At either location, the process is similar to that operating in the tube support plate crevices, with the creation of highly caustic or acidic conditions in the crevice because of local boiling and concentration effects. ODSCC/IGA can also occur in the sludge-pile region above the RTZ. The situation here is very similar to that presented at the tube support plate crevices filled with corrosion product and sludge. These cracks are commonly axial, but more complex multidirectional cracking has been reported in Belgian plants [15]. Also, secondary-side ODSCC and IGA in the free-span region have been observed a number of times over the years [16]. A particularly troubling recent trend has been the increasing occurrence of circumferential cracking at the RTZ on both the primary and secondary sides. Such circumferential cracks normally require plugging or sleeving upon detection, since they are difficult to reliably size, the threshold of detection for these cracks is greater in terms of size than for axial cracks, and their growth rates are difficult to predict [17]. Both axial and circumferential cracking have been observed at dented TSP locations in several of the same plants that have reported circumferential RTZ cracking. From the theory of pressure vessels, it can be inferred that axial cracks are more dangerous as the circumferential hoop stress causing axial cracking is double of axial stress causing circumferential flaw. Hence, simulation of axial cracking and necessary engineering related to material and design of the component will suffice fail-safe criteria for safe operation of power plant with minimal failure of SG tubes. Additionally, flow induced vibration causes other type of damages to SG tube involving cyclic loading. The damage caused due to synergistic effects of residual stress generated due to difference in temperature at inner and outer surface of the tube, corrosion and flow induced vibration can lead to gradual thinning and reduction in load bearing capacity of the tube and ultimately formation of tiny cracks causing leaking and catastrophic failure through propagation of cracks.

From the review of literatures, it is evident that much progress has been made for addressing the corrosion and flow assisted vibration problems associated with degradation of SG tubes. That led to evolution of better and far better tube material, incorporation of proper fixing arrangements at select places and control of water chemistry for minimization of damage due to corrosion. However, the fracture aspect of the tubes used as a component does not get so much significance in open literature. Perhaps this is so because the unusual geometry of the tube that prevents fabrication of standard test specimens from the component. Thus, flaw tolerance of SG tube as a component is never quantified to the best knowledge of the authors. Flattening of curved surface of the thin tube can lead to incalculable variation in residual stress and alteration of microstructure and thus correct estimate of fracture data cannot be achieved. A number of attempts were made in the past [18], for fracture property evaluation for axial cracking of thin tubes; Pin-Loaded Tension [19], Vallecitos Embedded Charpy [20], X-Specimen [21], Internal Conical Mandrel [22], Double-Edge Notched Tension [23] and Burst Test [24] are only a few to name. Out of these, all the techniques except the Internal Conical Mandrel (ICM) and the Burst Test (BT) followed the conventional procedure of evaluating J integral values from load-displacement curves. All these non-standard test methods have specific merits and demerits in their application to material testing and thus they are meant for specific use as per user requirements. From the earlier studies, it can be concluded that for thin-walled tubing, no single value of fracture toughness exists.

However, it does appear possible to obtain a useful toughness value that is appropriate for a specific application, if the technique specimen geometry and local stress-strain conditions closely models the application. Thus for SG tube also, as it possesses a unique tube geometry specific to its application, extrapolation of test data of earlier done test for similar material or geometry is of no use unless and until the tube itself can be tested. In recent past, the authors adapted test method called pin-loading tension test (PLT) originally developed by Grigoriev et al. [19, 25] and made necessary customizations to the test set up [26-31] for calculating J-R curves for cladding tubes used in Indian PHWR and BWRs. The authors have already established that use of proper geometric functions, such as η and γ functions are essential for proper estimate of J integral and using load normalization method [28-30] and also with load separation method [31], J-R curves for cladding tubes of Indian reactors are derived by the authors. The current work attempts to implement the same method for finding J-R curve for an axially cracked SG tube made of Fe-Cr-Ni alloys (popularly known as Incoloy-800) used for steam generation in Indian PHWRs. Although the tube is exposed to higher temperature during service, estimation of axial crack resistance of the tube at room temperature will reasonably provide meaningful conservative data from the point of view of safety of the component. The as-received tube is used for fabricating specimens and as per the specimen geometry the PLT fixture is customized for testing. Using the test set-up, experiments are carried out along with finite element (FE) analysis for determination of all required geometric functions for calculation of stress intensity factor (SIF), and η and γ functions for calculation of J integral for an axially cracked tubular specimen. With the fracture toughness test data, using the geometric functions, J-R curve for cracked specimens are calculated using load normalization method. Fractographic study of the fracture surface is also done to characterize the mechanism of axial cracking of SG tube.

This paper is divided into five sections. In Section II, the experimental details are discussed. The analytical framework adopted for analysis of experimental data and FEM analysis for calculation of geometric functions for an axially cracked SG tube specimen are mentioned in Section III. Results are critically discussed in Section IV followed by concluding remarks in Section V.

II. EXPERIMENTAL

A. Material

SG tube made of Incoloy-800 with chemical composition (wt %): Fe-45.97, Ni-32.29, Cr-19.87, Mn-0.59, Al-0.42 and Ti-0.49 as major alloying elements is chosen for the present study. The component having an inner dia. of 14 mm and wall thickness of 1 mm and length of about 3 meter is used as SG tube for generating steam from the heat generated by nuclear fission in the core of Indian pressurized heavy water reactor (PHWR). In Fig.1, the optical and scanning electron micrographs are shown. In the optical micrograph, [Fig. 1 (a)], signature of heavy amount of cold work (the elongated grain shown with arrow) can be noticed from the austenitic grain structure. There are annealing twins across the grains because of stress relieving after cold working and red colored rectangular precipitates are also seen throughout the matrix. Later through SEM [Fig. 1 (b)] and EDS the precipitates are identified as TiN and TiC. These particles provide coherency strengthening to the matrix and enhance fracture toughness of the material.

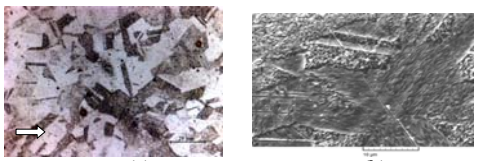

(a) (b)

Fig. 1 (a) Optical micrograph and (b) Scanning electron micrograph of Incoloy-800

B. Details of Specimen and Fixture

The detailed design of specimen and fixture for PLT test has been elaborated in the references [26-31]. In Fig. 2, at the left side the physical appearance of a PLT specimen fabricated from the SG tube through EDM wire cutting is shown. As can be seen, the specimen is basically a 13 mm long section of the large tube with four diametrically opposite coplanar notches machined, i.e. two at each end. At one end, the notch thickness is maintained as low as possible (typically 0.15 mm) and at the other, the notches are basically rectangular slots with dimension 2 mm × 0.5 mm. It is critical while machining to ensure all four notches to remain on a plane across the tube diameter. Two different sets of specimens are fabricated. One set consists of seven specimens with the thinner notch length varying from 1 mm to 7 mm with an interval of 1 mm. the other set has several specimens with constant thinner notch length of 1.5 mm.

At the middle of Fig. 2, the appearance of the PLT fixture is shown. Nimonic-90 is used for fabrication of the fixture. The fixture essentially contains two symmetric split halves. Each split half is a combination of a semi cylindrical mandrel and a rectangular block. The diameter of the mandrel is determined by the inner dia. of the thin tube under consideration to ensure a good transition fit. The split fixture halves when being put together form the cylindrical mandrel for accommodation of the specimen as shown in Fig. 2. At the left end of the fixture assembly, a small hole is formed at the joint for insertion of a small pin (shown just at the right of the fixture at Fig. 2) for determining the mutual rotation axis of the split fixture halves when loaded. The position of the rectangular slots of the specimen actually matches with the position of the pin when the specimen is assembled with the fixture. At further extreme left of the fixture, a grove is seen for fixing of a clip to preclude axial shift of the specimen under tensile load. Hence, it is evident that the wider rectangular slots provided at one end of the specimen is to avoid material cramping under compressive load. At the rectangular blocks of the fixture halves two through and through holes are noticed for insertion of pins (shown at extreme right of Fig. 2) for mode I type [32] loading of the specimen-fixture assembly, analogous to a CT specimen. At extreme right of the fixture, a pair of knife edges is machined for insertion of a clip gage for measuring crack opening displacement (COD). As can be seen from Fig. 2, the fixture has two important measurements: *W* and *b*. *W* is the horizontal distance between the centre of pin determining mutual rotation axis of the fixture halves and the vertical line joining centres of the two holes through with the test set up is loaded. In the present case, as the specimen length is 13 mm, *W* is fixed as 19 mm in the fixture design. Again, *b* is the horizontal distance between vertical line joining centres of the two holes through with the test set up is loaded and the interface between the rectangular and semi-cylindrical part of the fixture half. In the present case, *b* is 8 mm. If the PLT test set-up is compared with a standard CT specimen it can be inferred that the specimen-fixture assembly has a width (*W*) of 19 mm and the effective crack length of the specimen would be its original crack length plus 8 mm (i.e. *b*). Apart from these, suitable clevis grips are fabricated for attaching the PLT test set-up with a universal testing machine.

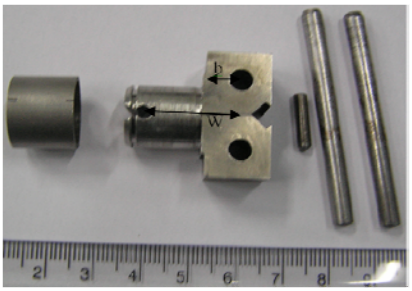

Fig. 2 Specimen, fixture and pins used for experiment

C. Testing of Specimens

Using a servo hydraulic universal testing machine, all testing are performed. The set of seven specimens with notch lengths 1-7 mm are pulled to fracture with a pull rate of 0.2 mm/min [Fig. 3(a)]. The load-COD data are digitally recorded for further analysis.

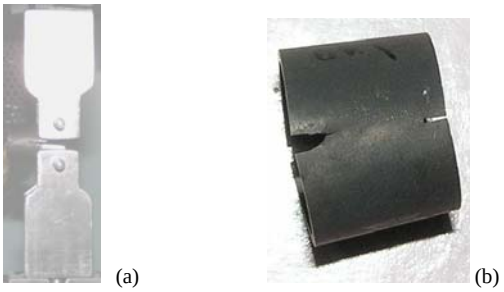

(a) (b)

Fig. 3 (a) Mode I loading of a PLT specimen with test set up (b) Appearance of a cracked PLT specimen after heat tinting and before cleave opening

For the specimens with constant initial notch length of 1.5 mm, they are initially subjected to cyclic loading with a decreasing load steps and the region ahead of notch tip is monitored using a travelling microscope till a fatigue crack of ~1.5 mm is developed at both sides of the specimens. Thereafter, nine best specimens are pulled up to fracture with a pull rate of 0.5 mm/min up to different extent of total displacements beyond maximum load ranging from 2.5 mm to 4.4 mm. the cracked specimens are then subsequently heat tinted within a furnace by heating at 500^{O}C for an hour [Fig. 3(b)] and then again subjected to cyclic loading for final cleave opening. The crack length of all specimens at both sides is measured using a stereomicroscope with the method of nine point averaging (Fig. 4). A solid block with thickness of 13 mm is drilled with a hole with dia. same as the inner dia. of SG tube and is attached with the PLT test set-up and subjected to load controlled pulling up to an appreciable load within elastic limit to find the machine compliance and that data are used later to subtract the contribution of machine from total displacement data to find the actual load-line displacement for each of the nine PLT specimens. A detailed fractographic study has also been performed under scanning electron microscope (SEM) for predicting suitable mechanism of axial cracking of Incoloy-800 SG tubes.

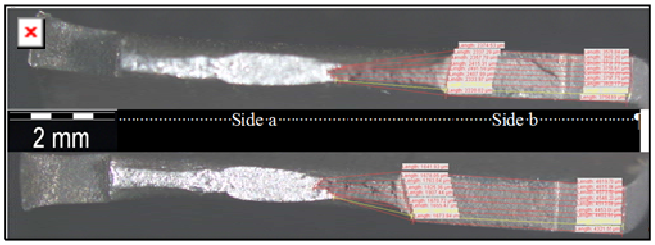

Fig. 4 Measurement of crack lengths of a specimen at both sides before and after fracture toughness testing

III. ANALYTICAL FRAMEWORK

A. *Determination of Geometric Shape Function, f(a/W) for Calculation of SIF*

The elastic compliance for each of the seven specimens with notch lengths ranging from 1 mm to 7 mm is first determined from the initial linear part of the Load-COD curves. Compliance is basically the inverse of the slope of the linear part. The compliance data are plotted against normalized crack length of the specimens. If a is the notch length, then normalized crack length (*a/W*) is given by (a+*b*)/*W*, where *b* and *W* are the parameters pertaining to fixtures and their values have already been mentioned in section IIB. The details of the two independent approaches adapted for finding *f(a/W)* for calculation of stress intensity factor (SIF) due to axial crack has already been discussed in ref. [26-27, 29]. From the concept of strain energy release rate [33], it can be shown that for an axially cracked tube,

$$K_I = \frac{P}{2t\sqrt{W}} f(a/W) \text{ and } f\left(\frac{a}{W}\right) = \left[\frac{1}{2} tE \frac{dC}{d(a/W)}\right]^{0.5} \quad (1)$$

where, K_I is mode-I SIF, *P* is load, *t* is tube wall thickness, *f(a/W)* is the geometric shape function for considering effect of finite size specimen geometry, *E* is elastic modulus, and *C* is specimen compliance. The success in finding *f(a/W)* depends on the accuracy in differentiating *C* w.r.t. *a/W*, as seen in Eq. (1). In approach 1, *C* is plotted against *a/W* and is fitted in the form of a polynomial function in *a/W* and subsequently it is differentiated w.r.t. *a/W* using power law. This method is less accurate as error associated with numerical differentiation is more. In approach 2, proposed by Ryder et al. [34-35], *C* and *W* are first analytically correlated using a function *Z* to express $\frac{dC}{d(a/W)}$ completely in the form of *a/W*:

$$\frac{d(CEt)}{d(a/W)} = \exp[\exp(g(a/W))]\exp(g(a/W))g'(a/W), \quad (2)$$

where, $g(a/W) = e + (v-e)[-\ln(1-a/W)]^{1/k}$ and, $g'(a/W) = \frac{v-e}{k}[-\ln(1-a/W)]^{(1/k)-1}\left[\frac{1}{1-a/W}\right]$

Then, with suitable linear fitting of $\ln(\ln(\ln(CEt + 2.71828)))$ vs. $\ln(-\ln(1-a/W))$ and imposing the necessary boundary conditions, the constants *v*, *e*, and *k* are found out to express *f(a/W)* in terms of *a/W*:

$$f(a/W) = \sqrt{\frac{\exp[\exp(e + (v-e)[-\ln(1-a/W)]^{1/k})]\exp(e + (v-e)[-\ln(1-a/W)]^{1/k})\frac{v-e}{k}}{[-\ln(1-a/W)]^{(1/k)-1}\left[\frac{1}{1-a/W}\right]}} \quad (3)$$

With this method, a more accurate measure of *f(a/W)* can be found, as the nature of the function is purely analytic. Using the function *f(a/W)*, SIF is determined for the axially cracked tube and using that, J_{el}, i.e. elastic part of J integral is determined using the relation, $J_{el} = K_I^2/E$ for plane stress loading condition [32].

Finite element (FE) analysis is also adapted for finding *f(a/W)* for an axially cracked SG tube for the same test set up as used in experiment. The details of the procedure are described in ref. [26-27, 29-30]. A 3D FE analysis of the SG tube specimen along with the loading mandrel has been carried out (Fig. 5). Considering symmetry, only a quarter modelling is done and the crack tip is defined with suitable mirror boundary conditions. Mesh is sufficiently refined to define the crack tip and avoidance of sharp stress gradient at the vicinity of crack front and subsequently merged to bigger elements away from the crack region considering economy in resource during simulation. The FE discretization is performed using 20-noded iso-parametric brick elements with 3×3×3 gauss point integration (full integration scheme). Total seven different meshes are created considering notch lengths ranging from 1 mm to 7 mm. Elastic-plastic analysis with von-Mises yield surface and isotropic plastic hardening constitutive equations have been carried out. A prescribed displacement is applied at the end of the mandrel in y-direction. For evaluation of stress intensity factor K_I, the displacement extrapolation method has been used. Neglecting higher order terms, the expression for K_I with respect to v (opening displacement ahead of crack tip) can be written for plane stress condition as

$$K_I = \frac{E}{4}\sqrt{\frac{2\pi}{r}}\text{v} \quad (4)$$

In Eq. (4), *r* is the distance of the material point from the crack tip where the displacement v is evaluated from the FE analysis results. For an applied displacement of 0.01 mm, the stress intensity factor K_I has been evaluated as a function of *a/W* at different points across the thickness of crack front. From the result, *f(a/W)* is derived using Eq. 1. The result thus obtained is compared with experimental results in section IV.

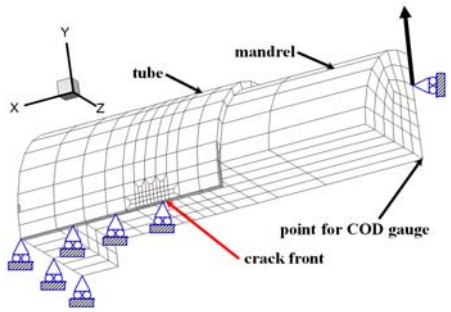

Fig. 5 FE mesh of the quarter-symmetric model of the SG tube specimen with loading setup with boundary and loading conditions

B. *Determination of η and γ Function for Calculation of J_{pl} from Experimental Data*

η and γ functions are important in calculation of plastic part of J integral, i.e. J_{pl} and as a correction term for calculation of J_{pl} for a growing crack respectively. The importance of the terms can be observed with the following equations:

$$J_{pl} = \frac{\eta A_{pl}}{b_0 B}, \text{ and}$$

$$J_{pl(i)} = \left[J_{pl(i-1)} + \left(\frac{\eta_{(i-1)}}{b_{(i-1)}} \right) \frac{A_{pl(i)} - A_{pl(i-1)}}{2t} \right] \left[1 - \gamma_{(i-1)} \frac{a'_{(i)} - a'_{(i-1)}}{b_{(i-1)}} \right] \quad (5)$$

where, A_{pl} is the area under load-load line displacement curve, considering only plastic (i.e. non linear part) part, b_0 is the length of initial unbroken ligament, a is gross crack length, B (i.e. $2t$) is the gross specimen thickness, and the respective terms with subscripts denote the same corresponding things for a growing crack at i^{th} and $(i\text{-}1)^{th}$ steps. η function can also be defined as a non-dimensional parameter that takes into account of the effect of geometry and loading condition at the crack-tip of a cracked specimen on the differential energy that is required for crack growth, whereas γ function can also be defined as a non-dimensional parameter that accounts for correction in the J-integral calculation due to crack propagation, which is otherwise defined for a stationary crack. The η and γ functions can be derived as a function of limit load F_L *(a/W)* [36, 37]:

$$\eta = -\left(1 - \frac{a}{W}\right) \frac{1}{F_L} \frac{\partial F_L}{\partial (a/W)} \text{ and } \gamma = \eta - 1 - \left(1 - \frac{a}{W}\right) \frac{1}{\eta} \frac{\partial \eta}{\partial (a/W)} \quad (6)$$

For evaluation of the above η and γ functions, the limit load solutions are required for the cracked tubes with different notch lengths as discussed earlier. The following material properties (of Incoloy-800 at room temperature) have been used for elastic-plastic FE analysis, i.e., yield stress of 210 MPa; ultimate tensile stress of 500 MPa. The limit load has been obtained as the starting load (corresponding to the applied displacement) at which the remaining ligament of the specimen goes into plastic deformation. The limit load reduces with increase in *a/W* ratio. From the limit load as a function of *a/W*, η and γ functions are derived using Eq. (6).

C. *Calculation of J-R Curves from Experimental Data Using the Derived Functions*

The details of this calculation have already been discussed in ref. [27-30]. The corrected load-line displacement for cracking of specimens is first accurately estimated by subtracting displacement due to machine compliance from total displacement and from load-corrected load-line displacement curve, the plastic area for all specimens are estimated (Fig. 6). From the nine-point averaging results under stereomicroscope, the initial unbroken ligament (b_0), initial and final crack length (a_0 and a_f) and the extent of crack extension (Δa) are also known. Using Eq. (5), the J_{pl} for all specimens are estimated and the required value of η is used from the derived η function using Eq. (6). J_{el} is also estimated for all specimens using the experimentally derived *f(a/W)*. J integral for all specimens are found by adding J_{el} with J_{pl} and the J-Δa curve for multiple specimens is constructed by plotting J with corresponding Δa.

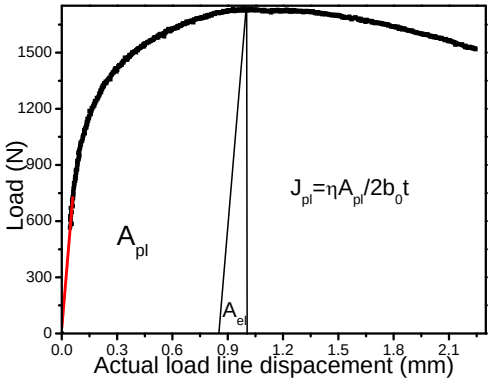

Fig. 6 Calculation of plastic area for a data point for finding *Jpl*

For finding J-R curves for each specimen using single specimen approach, the load normalization procedure included in ASTM standard E 1820 [38] is used. Basically, in this method, estimate of crack growth is done from the load-load line displacement data after normalization with suitable curve fitting. For doing that, first, all load (P) and load-line displacement (v) data points are normalized starting from initial point up to P_{max} using the relations:

$$P_{Ni} = \frac{P_i}{2tW\left[\left(W - a'_{bi}\right)/W\right]^{\eta}}, \text{ and } v'_{pli} = \left(v_i - P_i C_i\right)/W,$$

where $$a'_{bi} = a'_0 + J_i / 2\sigma_Y \quad (7)$$

In Eq. (7), P_{Ni} denotes the normalized load corresponding to load P_i for the i^{th} point of the curve (Fig. 6). Similarly, v_{pli} denotes the corresponding plastic displacement for the i^{th} point. Note that using the specimen compliance, the elastic displacement has already been subtracted from total displacement for finding the plastic displacement before normalization. This is because, plastic collapse occurs much before actual crack growth. The term a'_{bi} is the blunting corrected crack size at the i^{th} data point and its estimate involves calculation of J integral for all data points based on initial gross crack length (a_0) and $2\sigma_Y$ is basically sum of YS and UTS of the material. The final load-load line displacement data point corresponding to the end of fracture toughness test or end of crack front under stereomicroscope are also normalized using the actual measured crack length (a_f). After plotting P_{Ni} against v_{pli}, (Fig. 7), a tangent is drawn from the final point over the remaining data points and the data points if any residing at the right hand side of the tangent are discarded; data points with v_{pli} <0.001 are also discarded. The remaining data points are fitted with the following equation:

$$P_N = \frac{a + b v'_{pl} + c v'^2_{pl}}{d + v'_{pl}} \quad (8)$$

where, *a*, *b*, *c* and *d* are fitting coefficients found through the method of least squares. This practice is individually made for all the nine specimens and the nine different sets of fitting constants thus obtained are tabulated. Using Eq. (8), P_{Ni} for v_{pli}>0.002 up to the maximum value for each case with an interval of Δv_{pli}=0.001 is found out and then using Eq. (7), necessary modification in the values of $a_{bi}^{'}$s is done to get accurate estimation of crack growth for each specimen. Once, all intermediate crack lengths between a_0 and a_f are known, J_{pl} is calculated for each data point using Eq. (5) and J_{el} is also calculated for each point and thus J-R curves for each of the specimens have been derived.

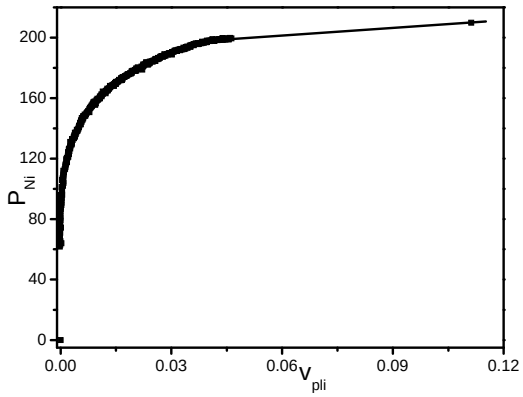

Fig. 7 Fitting of normalized data points using tangent through the final point on remaining curve for estimation of crack growth

IV. RESULTS AND DISCUSSION

A. *Experimental vis-à-vis FEM Results for Determination of Geometric Factors*

The load-COD response for all the seven specimens with different notch lengths is shown in Fig. 8. Obviously, compliance of specimen increases with increase in notch length and that fact is reflected in Fig. 9. The normalized notch length for each specimen is calculated with the method described in section IIB. The compliance function, as obtained through polynomial fitting is as following:

$$C(mm/N) = -0.00268 + 0.01795(a/W) - 0.03809(a/W)^2 + 0.02794(a/W)^3 \quad (9)$$

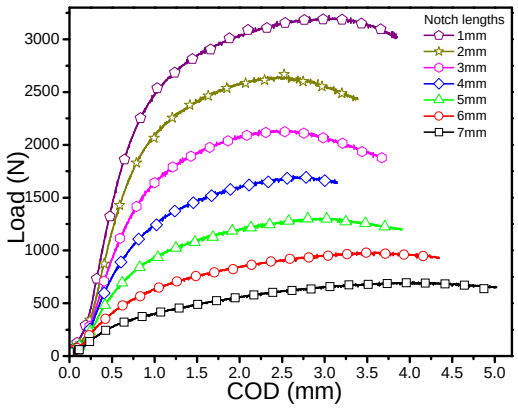

Fig. 8 The load-COD response of all seven PLT specimens showing decrease in stiffness with increase in notch length

This function is also used later in Eq. (7) for finding v_{pli} in the displacement normalization procedure for finding plastic part of displacement. For calculation of *f(a/W)*, *E* of value 195 GPa [39] is used and *t*=1mm [Eq. (1)].The result obtained by adapting approach 1 (described in section IIIA) is graphically shown in Fig. 10. The corresponding shape function expression is

$$f(a/W) = 0.47825 - 28.71231(a/W) + 107.55492(a/W^2) \quad (10)$$

With approach 2, when it is derived, the constants, *e*, *v* and *k* are found out to be 0, 1.5352, and 3.5714 respectively by linear fit for $\ln(\ln(\ln(CEt + 2.71828)))$ against $\ln(-\ln(1-a/W))$ and the result is graphically shown in Fig. 10. The corresponding shape function expression as per Eq. (3) is

$$f(a/W) = \begin{bmatrix} 0.44\exp\{\exp(1.54[-\ln(1-a/W)]^{0.28}\} \\ \exp(1.54[-\ln(1-a/W)]^{0.28}) \\ \{-\ln(1-a/W)\}^{-0.72}\{1/(1-a/W)\} \end{bmatrix}^{0.5} \quad (11)$$

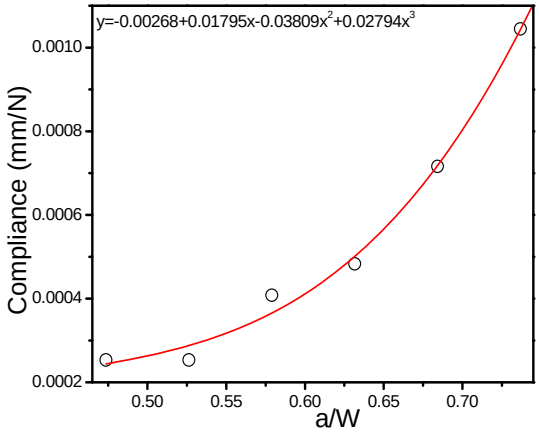

Fig. 9 The plot of compliance for the specimens from experiment with normalized notch lengths

With FEM, after doing the simulation in each case, the displacement of the nodes remaining both at inner and outer side is considered individually. The nodal displacement is plotted against square root of the distance from crack front up to the free end of the specimen and slope of the curve is used for calculation of SIF as per Eq. (4). After that *f(a/W)* is calculated using Eq. (1). The resultant values are plotted against *a/W* and graphically shown in Fig. 10 for both inner and outer nodes. The shape function results as obtained by all experimental and FE method are graphically compared in Fig. 10. Between 0.6 and 0.75 of the values of *a/W*, the experimental curves are found to match well with each other. Outside this band, for lower *a/W*, approach 1 is found to predict a higher *f(a/W)* value whereas approach 2 does the same for higher *a/W*. However, the curve for approach 2 is found to match well with the FEM findings for the highest *a/W* considered here unlike the curve for approach 1. Overall, also, FEM results show closer resemblance with the curve for approach 2 but the FEM result is always a little lower than the experimental findings. In fact, there is variance in FEM result if one considers the variation of SIF across the tube wall thickness and from Fig. 10, it is clear that the FEM result for inside surface of the tube is matching more closely with experimental findings. When the result is compared with earlier published results by authors [26, 27, 29] for zircaloy cladding tubes, it is found that unlike for CT specimens which has only one geometry parameter, i.e. specimen thickness, PLT specimens have two separately independent geometry parameters, i.e. tube diameter and wall thickness and thus, variation in *f(a/W)* expressions exists with variation in tube

geometry. In fact, in case of CT specimens, wall thickness is also normalized with specimen compliance (C) and material property, i.e. elastic modulus (E) and thus the expression for $f(a/W)$ becomes independent of specimen thickness. But such is not the case for PLT specimens and thus the geometric shape function, $f(a/W)$ is sensitive to tube geometry. This is important in essence as $f(a/W)$ is required for calculation of K_I and thus in turn it is used for calculation of J_{el} as well, as will be discussed while computing J from experimental load-displacement curve.

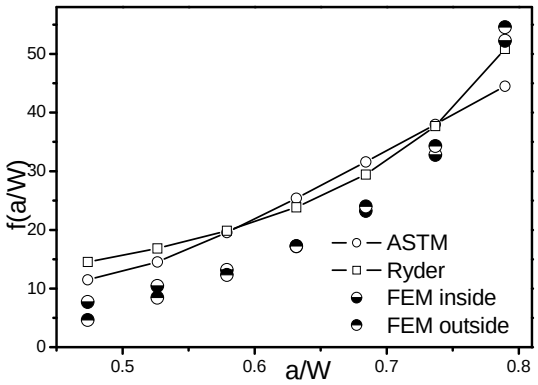

Fig. 10 Comparison of experimental and FEM results concerning the $f(a/W)$ expressions

The η and γ functions for axially cracked SG tube are derived using limit load formulations as described in section IIIB. Using Von Mises' yield criterion, the load i.e. limit load (F_L) at which gross yielding of remaining ligament of all the seven specimens happens is individually determined and F_L is plotted against a/W resulting in a linear fit. The function thus obtained is processed as per Eq. (6) to find expressions for η and γ functions and the results are graphically shown in Fig. 11. These functions are used for calculation of J_{pl} while deriving J-R curves to be discussed next. If one compares with the earlier similar results published by authors [27] it is evident that like $f(a/W)$, η and γ functions are also sensitive to tube geometry unlike for the case of CT specimens.

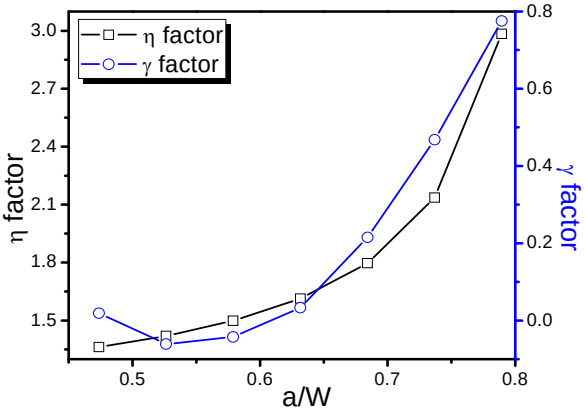

Fig. 11 η and γ functions as derived using limit load formulation

B. *J-R Curves Derived from Experimental Data Using the Geometric Factors*

For all the nine load-displacement curves, as obtained from the fracture toughness testing, the actual load line displacement is found by subtraction of contribution of load frame from the total load line displacements and the actual load-line displacements for all specimens are given in Table I. All specimens are stretched beyond maximum load to ensure occurrence of crack growth. It is interesting to note here that more or less, there is a strictly monotonic increasing trend in actual load-line displacement, consistent with the fact that more is increase in crack length, i.e. Δa, more will be the crack mouth opening. The initial crack lengths (a_0) prior to fracture toughness testing along with crack growth data (Δa), as measured under stereomicroscope for all specimens are furnished in Table II. The initial remaining ligament (b_0) for all specimens is determined by subtracting respective a_0 from 11 mm (note that although the total specimen length is 13 mm, for calculation of remaining ligament it is treated as 11 mm as there is a rectangular slot of dimension 2 mm×0.5 mm at the back end). Using the a_0/W values, the η value for all specimens are determined (Fig. 11) and using those values and the total plastic area under each of the load-actual load-line displacement curves (Fig. 6) is determined. Then using Eq. (5), J_{pl} is determined for all specimens. Similarly, from a_0/W data, J_{el} is determined for all specimens using Eq. (1) and (10). The respective J_{el} is added with J_{pl} to find J in each case and J is plotted with Δa to construct the J-R curve with multiple specimens as shown in Fig. 13 with other single specimen results. The multiple specimen result is not crack-growth corrected as information about crack growth at each data point which is not available and the basis of calculation is initial crack length of all specimens. The best fit that passes through the nine scattered points is also shown in Fig. 13.

TABLE I THE NINE FRACTURED SPECIMENS' TOTAL AND ACTUAL LOAD-LINE DISPLACEMENTS

Specimen name	Total load-line displacement (mm)	Actual load-line displacement (mm) due to specimen
Sp 1	2.5	1.61254
Sp 2	2.6	1.82781
Sp 3	2.7	1.95688
Sp 4	2.8	1.94896
Sp 5	2.9	2.07882
Sp 6	3.1	2.24255
Sp 7	3.3	2.58484
Sp 8	3.5	2.86549
Sp 9	4.4	3.79587

TABLE II INITIAL CRACK LENGTHS AND CRACK GROWTH DATA FOR ALL THE NINE SPECIMENS

Sp. ID	Initial crack length a_0 (mm)			
	Side a	Side b	Avg. value	a_0/W
Sp 1	3.07303	3.34331	3.20817	0.589903
Sp 2	4.17409	3.56381	3.86896	0.624682
Sp 3	3.87813	4.55537	4.21675	0.642987
Sp 4	3.52175	4.43842	3.98008	0.630531
Sp 5	3.95971	4.13339	4.04655	0.634029
Sp 6	4.47243	2.53881	3.50562	0.605559
Sp 7	4.29026	3.00666	3.64846	0.613077
Sp 8	4.46536	4.81428	4.63982	0.665253
Sp 9	3.74452	4.49057	4.11754	0.637765

Sp. ID	Crack growth Δ*a* (mm)		
	Side a	Side b	Avg. value
Sp 1	0.46131	0.62697	0.544146
Sp 2	0.55117	0.86538	0.708274
Sp 3	0.43690	0.60107	0.518984
Sp 4	0.82746	0.70108	0.764272
Sp 5	0.83436	0.771	0.802676
Sp 6	0.8192	1.31364	1.066421
Sp 7	1.13380	1.51243	1.323115
Sp 8	1.18888	0.96652	1.0777
Sp 9	2.35654	1.71967	2.038102

For constructing single specimen J-R curves for each of the specimens, the method described in section IIIC is adapted individually for each specimen. The fitting coefficients, obtained for Eq. (8) for each specimen is shown in Table III. Using the coefficients, all P_{Ni}-v_{pli} data points are forced to lie on the fitted curve, using Eq. (7) as described in section IIIC and the crack growth information for all the nine specimens are shown graphically in Fig. 12. Using the crack-growth information, instantaneous crack (a_i) for any specimen at i^{th} data point can be found out. Using that and η and γ functions from Fig. 11, J_{pli} is calculated for all specimens using Eq. (5). J_{eli} is also calculated using Eq. (1) and (10) as described above. Thus, crack-growth corrected single specimen J-R curve for all nine specimens are shown in Fig. 13.

The single specimen J–R curves of all the specimens are very close to each other due to their close a_0/W ratios and these results match well with multiple specimen result, with an exception: single specimen results are crack-growth corrected whereas multiple specimen result is not. That is why multiple specimen result is always slightly underestimated from single specimen results [28, 29]. As this range of a_0/W ratio is also recommended by ASTM standard [38], these J–R curves (i.e., the lower bound curve) can be used for structural integrity analysis of the tubes during postulated, abnormal or accidental loading conditions. For Δa = 0.2mm, the corresponding J is found out to be ~ 250N/mm. As these J–R curve results are for service-unexposed specimens at room temperature, it is sufficient to provide conservative estimate of crack resistance behaviour of a newly service-exposed SG tube with this data. As time passes, flow induced degradation factors cause impairment to the crack resistance property of the component. Thus, for a tube exposed to service for longer time, one may expect a less steep J–R curve, i.e. a curve with less J corresponding to the same Δa if compared with the current results.

TABLE III FITTING COEFFICIENTS FOR ALL SPECIMENS AFTER NORMALIZATION

Sp. ID	Fitting coefficients for Eq. (8)			
	a	*b*	*c*	*d*
Sp 1	1.25688	212.00175	139.6024	0.01064
Sp 2	0.93373	203.73286	221.26832	0.00935
Sp 3	0.85464	233.1169	36.93915	0.01059
Sp 4	1.02816	207.78017	232.3105	0.01035
Sp 5	1.14669	220.62493	175.48165	0.01185
Sp 6	1.26555	221.41865	52.01028	0.01191
Sp 7	1.52084	215.30451	1.60746	0.01291
Sp 8	1.5898	237.86989	104.65078	0.01412
Sp 9	2.04529	244.03809	-10.85575	0.01804

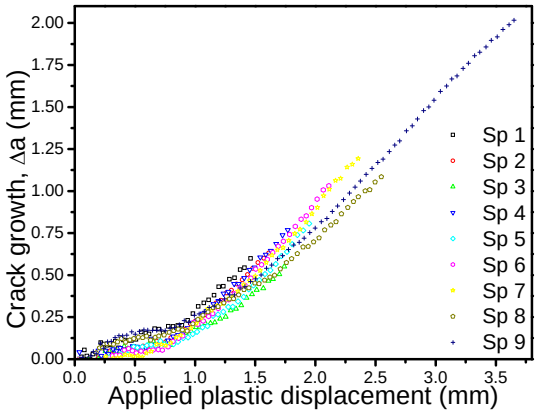

Fig. 12 Crack growth of all specimens after fitting of normalized curves

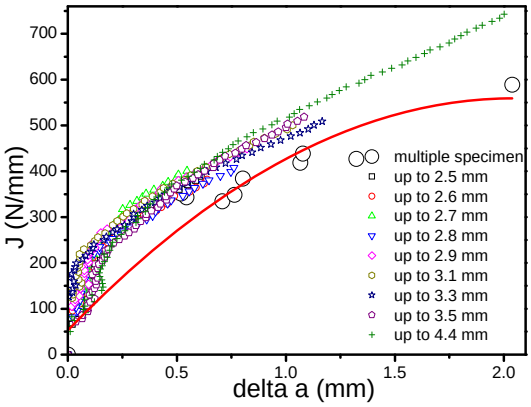

Fig. 13 J-R curve results for all specimens

C. Suggestion of Suitable Cracking Mechanism from Fractography

Scanning electron microscopy (SEM) has been done on the fracture surface (i.e. the region between pre-fatigue and post fatigue in Fig. 4) of a specimen. Although the specimen is oxidized through heat tinting for marking of the crack front, it did not cause any hindrance for fractography. The fracture surface as viewed in lower magnification (2000×) is shown in Fig. 14. The surface consists of great amount of dimples suggesting micro-void coalescence as the dominant fracture mechanism, as happened in the case of ductile fracture. If the optical microstructure (Fig. 1) is recalled, the matrix is infested with fine TiC and TiN intermetallics which has greater strength than the matrix. During loading, after yielding first de-cohesion takes place at the matrix-particle interface and that leads to micro-void formation. This phase corresponds to initiation of crack and customarily it can be marked on the J-R curve (Fig. 13) as the J value corresponding to Δa of 0.2 mm. from that point onwards, with an increase in SIF, local thinning of matrix between two or three micro-voids onsets leading to growth of micro-voids. The plastic deformation necessary for this process to occur leads to requirement of more energy and thus, a high slope in J-R curve is noticed. Ultimately, the local thinned region fails in cup and cone mode analogous to a tension specimen as shown in Fig. 16 (magnification: 10000×). The width and length of the cup shown in Fig. 16 is measured and the values are roughly 9 μm and 16 μm respectively. The apparently smooth fracture surface is actually quite rough as can be seen in Fig. 15 at higher magnification (5000×). This suggests that the phenomenon of axial cracking of Incoloy-800 tube at

room temperature is chiefly associated with huge plastic deformation and is transgranular in nature. If the nature of the fracture surface broken at service temperature differs with that in room temperature, then that may be a matter of future study with corresponding change in J for same Δa.

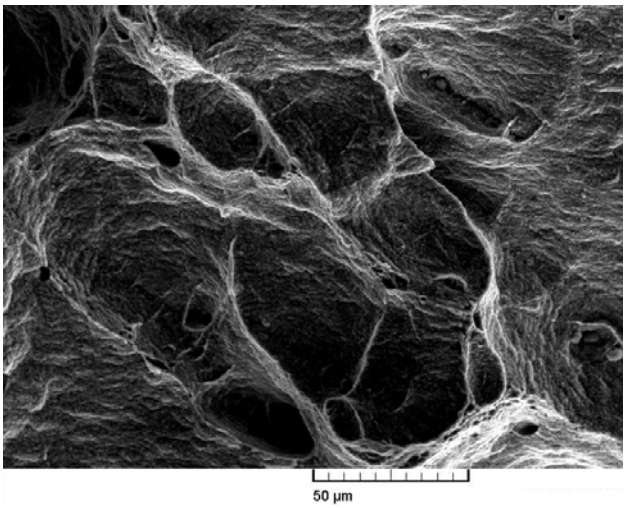

Fig. 14 SEM fractograph showing the fracture surface of SG tube material consisting of coalescence of micro voids forming dimples

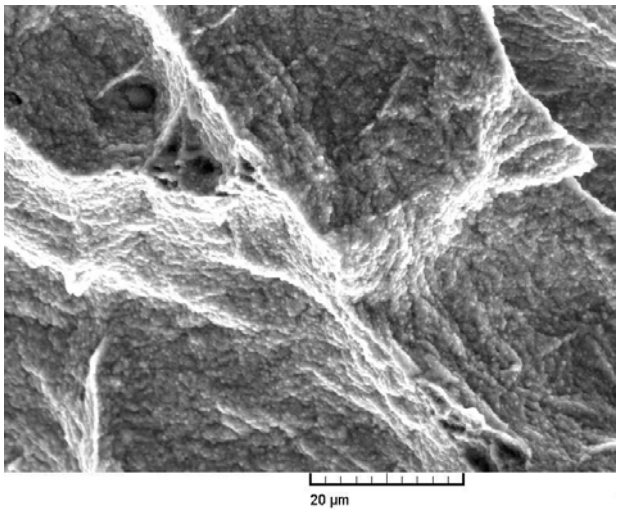

Fig. 15 SEM fractography with higher magnification showing the dull fracture surface corresponding to transgranular fracture with high prior plastic deformation

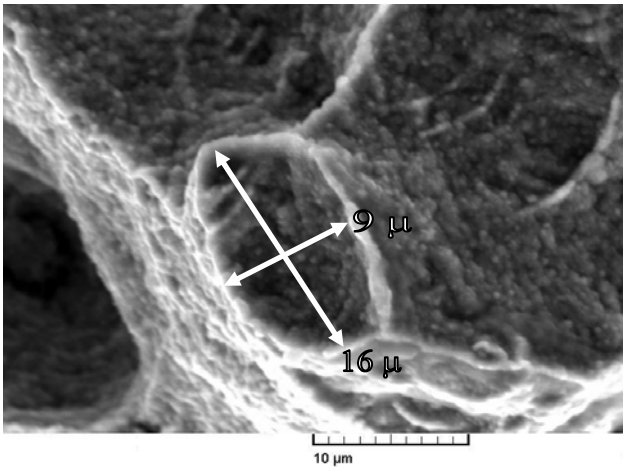

Fig. 16 SEM fractography showing a single ligament fractured in cup and cone mode resembling a sufficient local necking before complete fragmentation

V. CONCLUSIONS

Geometric shape function expressions for calculation of stress intensity factor of axially cracked SG tube made of Incoloy-800 for Indian PHWR is derived using experiment through PLT test and FEM analysis of the test set. The results are mutually consistent. The required functions for calculation of plastic part of J integral, both for a stationary and a growing axial crack for the same tube are derived using limit load formulation. Using those functions J–R curve of the axially cracked tube is derived after experiment using load normalization method and reproducibility is ensured. The probable mechanism of cracking is suggested through SEM fratography and micro-void coalescence is believed to be the dominant mechanism involved in such a ductile fracture. In the current study, the tests have been conducted at room temperature on a service unexposed tube. The fracture behaviour of service-aged SG tube specimens at room and higher temperatures will be a subject of future research.

ACKNOWLEDGEMENT

The authors are indebted to Dr. R. N. Singh, MMD, BARC and Mr. M. L. Rajput, NPCIL, Mumbai, India for arranging the SG tube used in Indian PHWR for carrying out the work and contribution of Dr. D. K. Aswal and Mr. S. Samanta of TPD, BARC, Mumbai, India for carrying out SEM fractography is also thankfully acknowledged.

REFERENCES

[1] http://www.nrc.gov/reading-rm/doc-collections/fact-sheets/steam-gen.html.

[2] S. K. Jain, “Role of Materials in Safe and Reliable Operation of Nuclear Power Plants”, Prof. Brahm Prakash Memorial Lecture, organized by The Indian Institute of Metals Bangalore Chapter, August 21, 2009.

[3] J. C. Fournel, “A Statistical Insight in the Suspected Relations Between PWSCC in R.T.Z. and IGASCC on TSPs”, paper #3 presented at the EPFU Workshop on Steam Generator Secondary Side IGA/SCC at Minneapolis, MN, on Oct. 14- 15, 1993.

[4] J. Stubbe, “Alloy 600 Primary Water SCC: a User's (Belgian Electricity Board) Point of View”, presented at the Alloy 600 PWSCC Experts Meeting, Arlie, France, April 6-9, 1993.

[5] C. S. Welty, Jr. and J. C. Blomgren, “Steam Generator Issues”, Proc. Fourth International Symposium on Environmental Degradation of Materials in Nuclear Power Systems-Water Reactors, pp. 1-27 to 1-36, Jekyll Island, GA, August 6- 10, 1989, National Association of Corrosion Engineers, Houston, TX (1990).

[6] C. O. Ruud and M. E. Jacobs, “Residual Stresses in Roller-Expanded Steam Generator Tube Transitions”, EPRI Report TR- 102355, Electric Power Research Institute, Palo Alto, CA (May 1993).

[7] J. A. Gorman and E. S. Hunt, “Critical Factors Assessment for U-Bend and Transition Cracking”, Proc.: 1985 Workshop on Primary-Side Stress Corrosion Cracking of PWR Steam Generator Tubing, EPRI NP-5158, Electric Power Research Institute, Palo Alto, CA (June 1987).

[8] P. Saint Paul and G. Slama, “Steam Generator Materials Degradation”, pp. 39-49 in Proc. Fifth International Symposium on Environmental Degradation of Materials in Nuclear Power Systems-Water Reactors, Monterey, CA, Aug. 25- 29, 1991, American Nuclear Society, La Grange Park, IL (1992).

[9] R. J. Kurtz, R. A. Clark, E. R. Bradley. W. M. Bowen, P. G. Doctor, and R. H. Ferris, Steam Generator Tube Integrity Program/Steam Generator Group Project, NUREG/CR-5 1 17, U.S. Nuclear Regulatory Commission, Washington, DC (May 1990).

[10] “Potential Failure of Westinghouse Steam Generator Tube Mechanical Plugs”, NRC Information Notice 89-33, U.S. Nuclear Regulatory Commission, Washington, DC (March 23, 1989).

[11] “Failure of Westinghouse Steam Generator Tube Mechanical Plugs”, NRC Bulletin 89-01, U.S. Nuclear Regulatory Commission, Washington, DC (May 15, 1989).

[12] E. Pierson and J. Stubbe, SCC Testing of Steam Generator Tubes Repaired by Welded Sleeves, pp. 697-705 in Proc. Sixth International

Symposium on Environmental Degradation of Materials in Nuclear Power Systems-Water Reactors, San Diego, CA, Aug. 1-5, 1993, R. E. Gold and E. P. Simonen, eds., The Minerals, Metals, and Materials Society, Warrendale, PA (1993).

[13] "Potential Failure of Steam Generator Tubes with Kinetically Welded Sleeves", NRC Information Notice 94-05, U.S. Nuclear Regulatory Commission, Washington, DC (January 19, 1994).

[14] J. P. N. Paine, S. A. Hobart, and S. G. Sawochka, "Predicting Steam Generator Crevice Chemistry", pp. 739-744, Proc. Fifth International Symposium on Environmental Degradation of Materials in Nuclear Power Systems-Water Reactors, Monterey, CA, Aug. 25-29, 1991, American Nuclear Society, La Grange Park, IL (1992).

[15] C. Leblois, "Belgian Steam Generator Experience: The Whole Picture", *Nucl. Eng. Int.*, Vol. 32, pp. 25-33, May 1992.

[16] K. Sweeney and M. Melton, "Free-Span IGA/SCC at the Palo Verde Nuclear Generating Station", EPRI Workshop on Steam Generator Secondary Side IGA/SCC, Minneapolis, MN, October 14- 15, 1993.

[17] "Circumferential Cracking of Steam Generator Tubes", NRC Generic Letter 95-03, U. S. Nuclear Regulatory Commission, Washington, DC (April 28, 1995).

[18] S. K. Yagnik, et al., "Round-Robin Testing of Fracture Toughness Characteristics of Thin-Walled Tubing", Journal of ASTM International, Vol. 5, No. 2, pp 1-21, 2008.

[19] Grigoriev, V., Josefsson, B., and Rosborg, B., "Fracture Toughness of Zircaloy Cladding Tubes," Zirconium in the Nuclear Industry: 11th International Symposium, ASTM STP 1295, E. R. Bradley and G. P. Sabol, Eds., ASTM International, West Conshohocken, PA, 1996, pp. 431–447.

[20] Edsinger, K., Davies, J. H., and Adamson, R. B., "Degraded Fuel Cladding Fractography and Fracture Behavior," Zirconium in the Nuclear Industry: 12th International Symposium, ASTM STP 1354, G. P. Sabol and G. D. Moan, Eds., ASTM International, West Conshohocken, PA, 2000, pp. 316–339.

[21] Hsu, H. H., Chien, K. F., Chu, H. C., Kuo, R. C., and Liaw, P. K., "An X-Specimen Test for Determination of Thin-Walled Tube Fracture Toughness," Fatigue and Fracture Mechanics: 32nd Volume, ASTM STP 1406, R. Chona, Ed., ASTM International, West Conshohocken, PA, 2001, pp. 214–226.

[22] Sainte Catherine, C., Le Boulch, D., Carassou, S., Ramasubramanian, N., and Lemaignan, C., "An Internal Conical Mandrel Technique for Fracture Toughness Measurements on Nuclear Fuel Cladding," J. Test. Eval., Vol. 34, No. 5, pp. 373–382, 2006.

[23] Bertsch, J. and Hoffelner, W., "Crack Resistance Curves Determination of Tube Cladding Material,", J. Nucl. Mater., Vol. 352, pp. 116–125, 2006.

[24] Oberländer, B. C., and IFE Kjeller, personal communication, Jan. 2000 and subsequent IFE report IFE/KR/F-2003/134, 2003.

[25] V. Grigoriev, B. Josefsson, A. Lind, and B. Rosborg "A pin-loading tension test for evaluation of thin-walled tubular materials" Scr Metall Mater vol. 33 no. 1, pp. 109–114, 1995.

[26] M.K. Samal, G. Sanyal, and J.K. Chakravartty, "An experimental and numerical study of the fracture behaviour of tubular specimens in a pin-loading-tension set-up", J Mech Eng Sci vol. 224 no. 1, pp. 1–12, 2010.

[27] M.K. Samal, G. Sanyal, and J.K. Chakravartty, "Estimation of fracture behavior of thin walled nuclear reactor fuel pins using Pin-Loading-Tension (PLT) test" Nucl Eng Des, vol. 240 no. 12, pp. 4043–4050, 2010.

[28] G. Sanyal, M.K. Samal, and J.K. Chakravartty, K.K. Ray, A.K. Suri, S. Banerjee, "Prediction of J-R curves of thin-walled fuel pin specimens in a PLT setup", Eng Fract Mech, vol. 78, no. 6, pp. 1029–1043, 2011.

[29] G. Sanyal and M. K. Samal, "Fracture behavior of thin-walled Zircaloy fuel clad tubes of Indian pressurized heavy water reactor", International Journal of Fracture, Vol. 173, No. 2, pp. 175-188, 2012.

[30] M.K. Samal, G. Sanyal, and J.K. Chakravartty, "Investigation of failure behavior of two different types of Zircaloy clad tubes used as nuclear reactor fuel pins", Engineering Failure Analysis, Vol. 18, no. 8, , pp. 2042-2053, 2011.

[31] M.K. Samal, and G. Sanyal, "A load separation technique to evaluate crack growth and fracture resistance behavior of thin-walled axially-cracked tubular specimens", J Mech Eng Sci, vol. 226 no. 6, pp. 1447-1461, 2012.

[32] T.L. Anderson, Mechanics Fracture. Fundamentals and applications, 2nd ed.. CRC Press, Inc.; 1995.

[33] V. Grigoriev, R. Jakobsson., "Application of the pin loading tension test to measurements of delayed hydride cracking velocity in zircaloy cladding" SKI Rapport 00:57, Studsvik Nuclear AB, SE-611 82 Nyköping, Sweden, November, 2000.

[34] J.T. Ryder, G.E. Browie, D.E. Pettit, "Recent considerations in experimental compliance calibration of the WOL specimen", Eng Frac Mech vol. 9, pp. 901–923, 1977.

[35] T.V. Duggan, M.W. Proctor, L.J. Spence, "Stress intensity calibrations and compliance functions for fracture toughness and crack propagation test specimens" Int J Fatigue vol. 1, no. 1, pp. 37–47, 1979.

[36] N. Miura, G.M. Wilkowski, "J–R curves from circumferentially throughwall cracked pipe tests subjected to combined bending and tension -part i: theory and numerical simulation" J Press Vess Technol, Trans, ASME, vol. 120, pp. 406–11, 1998.

[37] N. Miura, G.M. Wilkowski, "J–R curves from circumferentially throughwall cracked pipe tests subjected to combined bending and tension-part ii: experimental and analytical validation" J Press Vess Technol, Trans, ASME, vol. 120, pp. 120:412–7,1998.

[38] ASTM Standard E 1820-01 "Standard test method for measurement of fracture toughness" ASTM, Philadelphia, PA, 03.01: pp. 1-21, 2000.

[39] www.specialmetals.com, "The story of the 'INCOLOY® alloys series,' from 800, through 800H, 800HT®".

Gopal Sanyal was born in the city of Kolkata, India on March 28 in the year 1981. He is an M. Tech. (Master of Technology) in Metallurgical and Materials Engineering from Indian Institute of Technology, Kharagpur, India since 2007.

He works as a Scientist in Bhabha Atomic Research Centre, Mumbai, India since 2005. He has been working on axial cracking of thin-walled tubes and has many journal publications and book chapters in his credit pertaining to his area of interest.

Mr. Sanyal got Homi Bhabha Award for securing no. 1 rank during training examination within Metallurgy discipline prior to posting at his current job location. During undergraduate student days he was a student member of Indian Institute of Metals (IIM).

Mahendra K. samal was born in the district of Jajpur, Orisha, India on May 3 in the year 1974. He is a PhD (Doctor of Philosophy) in Mechanical Engineering from the University of Stuttgart, Germany since 2007. In the year 2009, he also went to Ohio State University for post doctoral research.

He works as a Scientist in Bhabha Atomic Research Centre, Mumbai, India since 1996. He has immense depth of knowledge and can express his ideas well. He has plenty of areas for research and teaching, out of which finite element method, damage mechanics, online creep-fatigue monitoring, smart materials, crystal plasticity are only a few to name. He has a good amount of journal publications in his credit and edited many books, contributing very important input to scientific world.

Dr. Samal got many awards throughout his career. He received Homi Bhabha Award for ranking first among the mechanical engineers during training before absorption to his workplace. During pursuing M. Tech., he received P.M. Natu memorial prize and Ashok Chaturvedi memorial prize for ranking first in the Mechanical Engineering department of IIT Bombay. He was also selected for DAAD fellowship for carrying out Masters thesis at Technische Universität Darmstadt, Germany. He is an active teacher in Indian Nuclear Society (INS) and has affiliation with many other professional bodies.